The International Journal of Advanced Manufacturing Technology (2021) 114:3285–3299
https://doi.org/10.1007/s00170-021-06949-z

ORIGINAL ARTICLE

Milling force model prediction considering tool runout with three-teeth alternating disc cutter

Yang Cheng [1] · Shi Yaoyao [1] · Xin Hongmin [1,2] · Zhang Nan [1]

Received: 13 November 2020 / Accepted: 16 March 2021 / Published online: 24 April 2021

Abstract

Disc cutter has a large diameter and more teeth, and obvious tool runout (δ_i) is produced during disc milling process, so the irregular distribution of cutting force is generated due to uneven distribution of cutting output per tooth (h_i^*) caused by tool runout. Therefore, the tool runout (δ_i) must be considered when milling force model of disc milling is established. In the paper, first, milling force model of disc milling is built with a three-teeth alternating disc cutter considering the tool runout (δ_i). Second, tool runout (δ_i) is measured by the dial gauge when the revolving speed of disc cutter is 1 r/min, then cutting output per tooth considering tool runout (h_i^*) is obtained by the formula between cutting output of each tooth (h_i) without considering tool runout (δ_i) and tool runout (δ_i). Third, the parameters of frictional angle (β_n), normal shear angle (ϕ_n), and shear yield strength (τ_s) in model coefficients are calibrated by orthogonal cutting experimental. Then, the predictive model of milling force is obtained. Last, the reliability verification experiment of model is conducted. The experiment results show that the model is with high efficiency and precision and the measured force and predictive force is in good agreement in amplitude and trend, which can be used in the study of milling force of disc milling.

Keywords Milling force · Model prediction · Disc milling · Blisk · Tool runout

1 Introduction

Blisk is the key part of aero-engine with narrow channel and varying curvature, which is almost made of difficult-to-cut materials such as titanium alloy and high-temperature alloy, so the manufacturing is faced with many difficulties. In present, CNC milling is the main machining method, and plunge milling and side milling are adopted, which leads to low processing efficiency, so the demand of mass production of aero-engine is restricted seriously. In order to resolve the problems, multi-milling process is put forward. There are three steps involved in multi-milling: first, disc milling is used to groove and remove most of the margin of the channel, which is a rough machining. Then, plunge milling is available to expand the size of groove, further forming the surface of the channel. Last, side milling is applied to remove the corner and angle on the channel's surface, which belongs to semifinishing [1]. Milling force is large during disc milling process compared to plunge milling and side milling, which has an important effect on cutting vibration, surface quality, tool wear, and cutting heat, so the accurate prediction of milling force is critical to control the milling performance and understand the milling mechanics during disc milling process.

Many scholars have carried out some researches on milling force model prediction and accumulated a lot of achievements. Feng [2] presents an approach to determine the polynomial cutting force coefficients; the least square regression method is utilized in the cutting coefficient evaluations; verification experiment results show that the measured force agrees well with the predicted force, which demonstrates the effectiveness of this approach. Based on the idea of sculptured surface and combining micro-element milling force model and undeformed chip thickness mode, a force predictive model with arbitrary cutter axis vector and feed direction is established by Wei [3]; the results of simulations and experiments show that the model is with high efficiency and

✉ Xin Hongmin
xhm0330@163.com

[1] Key Laboratory of High Performance Manufacturing for Aero Engine, Northwestern Polytechnical University, Ministry of Industry and Information Technology, Xi'an 710072, China

[2] Hubei Key Laboratory of Power System Design and Test for Electrical Vehicle, Hubei University of Arts and Science, Xiangyang 441053, China

precision and the measured force and predictive force are in good agreement in amplitude and trend. Lu [4, 5] develops a micro-milling force model under cutting conditions considering tool flank wear effect based on a three-dimensional dynamic cutting force prediction model. The tool wear condition was obtained by finite element method. The results show that the proposed modified force analytical model could predict cutting force more accurately. A generalized mechanical model is proposed to predict cutting forces for five-axis milling process of sculptured surfaces by song [6]; a solid-analytical-based method is presented and extended to precisely and efficiently identify the cutter-workpiece engagements between the tool and workpiece. Experimental validations show that the model can be applied for an arbitrary mill geometry in multi-axis milling as well as three-axis milling and two-and-a-half-axis milling. The deflection deformation rule of tool under cutting force and the coupling relationship between cutting force and deflection deformation of tool are studied by Li [7]; flexible cutting force prediction model in the process of hole helical milling is built. Testing results show that the diameter error is reduced from 35 to 5μm after compensation, which greatly improves the processing precision. The relationship between feed velocity and cutting force is considered by Stemmler [8]; a model-based predictive controller manipulates the desired feed velocity of the machine with respect to the machine behavior, which shows good performance in the case of feed velocity references in time domain. A milling force model for micro-end-milling is established based on size effect of specific cutting force by Zhang [9]; the specific cutting force is calculated by milling force divided by milling area. The experimental results show that the specific cutting force increases with the decrease of the helical angle in the ox direction and oy direction and decreases in the oz direction due to the effect of helical angle. An improved theoretical dynamic cutting force model in metal matrix composites of micro-milling process is presented by Niu [10], which is modified and improved based on the conventional milling force model while taking account various factors including tooling geometries, material microstructure, size effect, and chip formation. Simulation results indicate that the improved dynamic cutting force model can predict cutting force accurately and reveal more details on cutting force variations. The theoretical milling force model for formed milling cutter is built based on the theory of metal cutting by Cai [11], and the working profile of curved switch rail is chosen as processing object in milling experiment; the study results provide theoretical basis for tool machine design and process parameter selection.

The tool runout is inevitable during machining process; it also impacts the milling force, so many scholars think the tool runout must be taken into account when milling force model is established. Guo [12] presents cutting force coefficient identification model which is related to the instantaneous chip layer thickness and axial position angle considering the cutter runout. The cutter runout parameters are obtained with instantaneous measured milling force of single of teeth. A large number of milling experiments under different processing parameters show that the cutting force coefficients and cutter runout parameter identification model can be effectively applied to five-axis ball-end milling. Based on space constraint method, force prediction model considering tool runout for five-axis flat end milling of inclined plane is established by Guo [13]; experiment and simulation results show that the spatial constraint method is simpler and more versatile than the cutter-workpiece engagement limitation method and the predicted force is in good agreement with measured force in both trend and amplitude. A new and generic instantaneous force model is developed by Zhang [14], in which the size effect is reflected in force coefficients and the tool runout effect is included in instantaneous uncut chip thickness. In the model, the real engagement is comprehensively identified under tool runout effect. The proposed force model can be obtained by only calculation of the average uncut chip thickness with inclusion of tool runout effect. Experimental results show that maximal peak errors of the forces are all less than 0.6%, which validates the efficiency and accuracy of the proposed model. An analytical force model considering tool runout for ball-end milling based on predictive machining theory is built by Fu [15], which regards the workpiece material properties, tool geometry, cutting conditions, and types of milling as input data. The model is verified by the published results and experimental data. Good agreement shows the effectiveness of model and highlights the importance of the tool runout on the force prediction. A systematic and analytical cutting force prediction model considering tool runout for plunge milling is proposed by Zhuang [16]. The real-time uncut chip thickness of different inserts is calculated with consideration of effect of tool runout. Verification experiment shows the quite good agreements with measured cutting forces, which proves the correctness and accuracy of the proposed model. The milling force model is established for micro-milling process considering tool runout by Li [17], and the cutting force with different tool runouts is analyzed. The model can help to judge surface quality that is affected by tool runout though the analysis of variation of milling force.

Disc milling is a new process method for blisk machining. There is a little research on milling force of disc milling. Xin [18] conducted a series of experiment to study milling force of disc milling, but the test block, cutting tool, and machine tool used in the experiment are far different from the actual processing environment, so the significance of the results is not obvious. Zhang [19] established a 3-D instantaneous cutting force model of disc milling for machining blisk considering tool runout, but in this reference, the tool runout of disc cutter is considered to be caused by tool axis offset, which means the tool runout is regular. However, there are some random manufacturing errors and installation errors because the disc

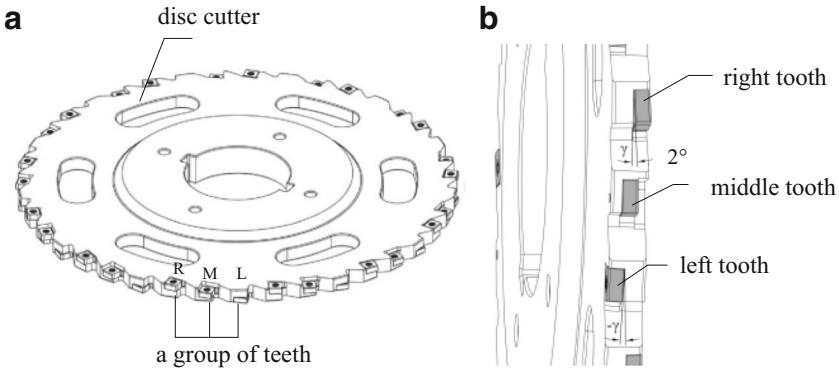

Fig. 1 Disc cutter. **a** The overall picture. **b** The enlarged view of the three-teeth alternating disc cutter

cutter has a big diameter and more teeth, which leads to the random tool runout instead of regular tool runout.

In the paper, first, the milling force model of disc milling is built with a three-teeth alternating disc cutter, and the random tool runout (δ_i) is taken into account. Second, the random tool runout (δ_i) is measured by the dial gauge when the revolving speed of disc cutter is 1 r/min; then cutting output per tooth (h_i^*) considering the tool runout (δ_i) is obtained by the formula between the cutting output of each tooth (h_i) without considering tool runout (δ_i) and the tool runout (δ_i). Third, the parameters of frictional angle (β_n), normal shear angle (ϕ_n), and shear yield strength (τ_s) in model coefficients are calibrated by orthogonal cutting experimental; then the milling force prediction model is gained.

2 Milling force model

2.1 The establishment of milling force model

In the study, a three-teeth alternating disc cutter is used, which has 39 teeth in all. Three teeth are in a group, which are arranged in order of right, middle, and left, so there are 13 right teeth, 13 middle teeth and 13 left teeth, respectively, as shown in Fig. 1. In order to avoid interference between the disc cutter and blisk channel during processing, the oblique angle is designed on blade groove along the thickness direction of the cutter body

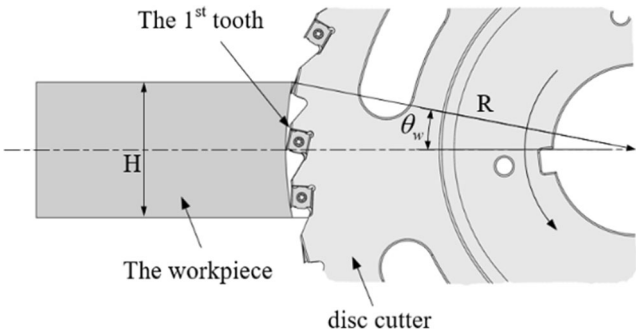

Fig. 2 Schematic diagram of disc milling

for the left tooth and right tooth, which is defined as cutting edge inclination angle; as shown in Fig. 1b, the angle of left side is marked $-\gamma$, the angle of right side is γ, and the value of γ is 2°. The design of oblique angle makes the cutting thickness of the disc cutter larger than the thickness of the disc cutter so as to avoid the interference between the disc cutter and blisk channel. In

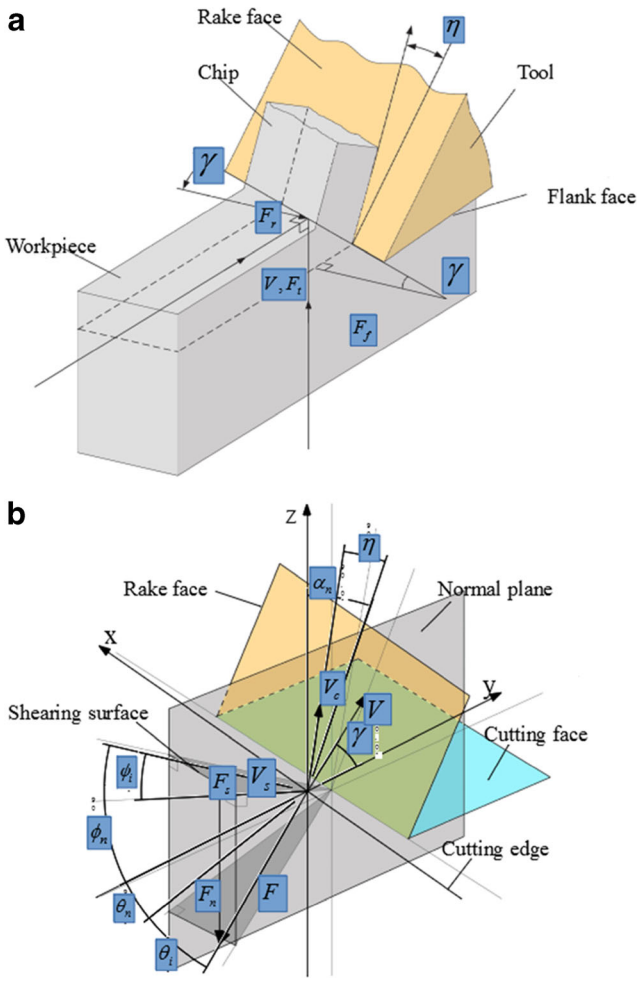

Fig. 3. The oblique cutting diagram. **a** The oblique cutting geometry diagram. **b** The geometry relation of oblique process

Table 1 The geometry of the disc cutter

Diameter(mm)	Number of teeth	Thickness(mm)	Body material	Blade material	Rake angle (°)	Relief angle (°)	Corner radius (mm)	Coating
420	39	15	32Cr2MnNIMo	Cemented carbide	8°	12°	0.8	TiAlN

addition, the left/right tooth is the oblique cutting because of the cutting edge inclination angle, and the middle tooth is the orthogonal cutting; orthogonal cutting can be regarded as a special case of oblique cutting, while oblique angle is 0°, so only oblique cutting needs to be considered in the paper.

In order to establish the milling force model of disc milling, the right tooth is defined as the first tooth, as shown in Fig. 2. The tip position of the first tooth is taken as the rotation starting point of the disc cutter when the tip of the first tooth is at the left of the disc cutter center. In addition, the positive direction of the disc cutter is that when the disc cutter rotates counterclockwise, as shown in Fig. 2.

A window function ($g_{Q,\ i}(\theta)$) is needed when milling force model is set up as shown in Eq. (1).

$$g_{Q,i}(\theta) = \begin{cases} 1 & \theta_{Q,st} \le \theta \le \theta_{Q,ex} \\ 0 & \text{else} \end{cases} \quad (Q = L, C, R) \tag{1}$$

In Eq. (1): L is left tooth, C is middle tooth, and R is right tooth. $\theta_{Q,\ st}$ and $\theta_{Q,\ ex}$ can be obtained by Eq. (2).

$$\begin{cases} \theta_{L,st} = \dfrac{(3i+1)\times 2\pi}{39} - \theta_w, & \theta_{L,ex} = \dfrac{(3i+1)\times 2\pi}{39} + \theta_w \\ \theta_{C,st} = \dfrac{(3i+2)\times 2\pi}{39} - \theta_w, & \theta_{C,ex} = \dfrac{(3i+2)\times 2\pi}{39} + \theta_w \\ \theta_{R,st} = \dfrac{3(i+1)\times 2\pi}{39} - \theta_w, & \theta_{R,ex} = \dfrac{3(i+1)\times 2\pi}{39} + \theta_w \end{cases} \tag{2}$$

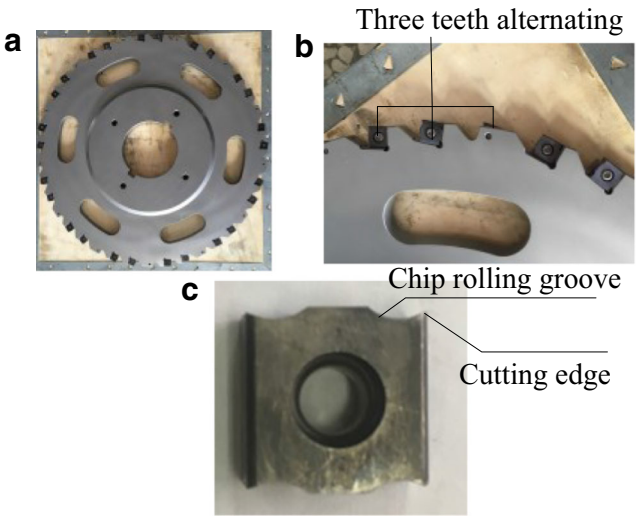

Fig. 4 **a** The disc cutter, **b** the blade, and **c** the distribution mode

In Eq. (2), i=1, 2, 3, , ,13. θ_w is the included angle between the center line and border line; the center line goes through the rotation starting point of the disc cutter and the center of the disc cutter, and the border line goes through the cut-in starting point of the workpiece and the center of the disc cutter, as shown in Fig. 2. θ_w can be achieved by Eq. (3).

$$\theta_w = \arcsin\frac{\mathrm{H}}{2\mathrm{R}} \tag{3}$$

In Eq. (3), H is the thickness of the workpiece, and R is the radius of the disc cutter.

The window function ($g_{Q,\ i}(\theta)$) is used to indicate whether the tooth participates in cutting. The value of $g_{Q,\ i}(\theta)$ is 1 when the tooth participates in the cutting, otherwise 0.

It shows that the i^{th} left tooth participates in cutting when $g_{L,\ i}(\theta) = 1$, the i^{th} middle tooth participates in cutting when $g_{C,\ i}(\theta) = 1$, and the i^{th} right tooth participates in cutting when $g_{R,\ i}(\theta) = 1$.

Based on the above theory, milling force prediction model is achieved, as shown in Eq. (4) (Altintas 2012).

$$\begin{cases} F_{Qt,i}(\theta) = g_{Q,i}(\theta) K_{Q,tc} b_i h_i^* \\ F_{Qf,i}(\theta) = g_{Q,i}(\theta) K_{Q,fc} b_i h_i^* \\ F_{Qr,i}(\theta) = g_{Q,i}(\theta) K_{Q,rc} b_i h_i^* \end{cases} \quad (Q = L, C, R) \tag{4}$$

In Eq. (4), $g_i(\theta)$ is the window function, which can be obtained by the diameter of the disc cutter and the thickness of the workpiece. b_i is the width of the cutting edge. h_i^* is cutting output of each tooth considering the tool runout, which can be obtained by the formula between the cutting output of each tooth (h_i) without considering tool runout (δ_i) and tool runout (δ_i).

2.2 Identification of coefficient and parameters in prediction model

2.2.1 Identification of coefficient in prediction model

The cutting velocity has an oblique or inclination angle γ in oblique cutting operation, and thus, the directions of

Table 2 The composition and property of blade

Material trademark	Content(wt.%)				Grain size (um)	Size (mm)
	W	Co	Cr	C		
YGB212	84.02	10	0.43	5.55	0.8	12.7×12.7×6

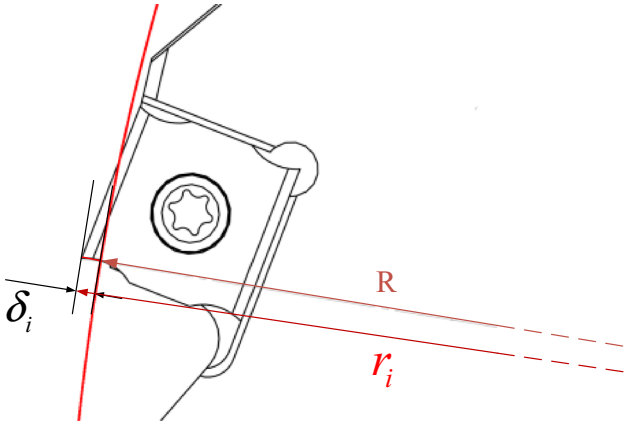

Fig. 5 The sketch map of tool runout of the disc cutter

shear, friction, chip flow, and resultant cutting force vectors have components in all three Cartesian coordinates (X, Y, Z). The geometric relation diagram of oblique cutting is shown in Fig. 3. It shows that F_t is tangential force; F_f is feed force; F_r is side force; F is the result of cutting force; F_s is shear force; F_n is normal force on shear plane; V is linear cutting speed; V_s is shear velocity; V_c is chip flow rate; γ is cutting edge inclination angle; η is chip flow angle; α_n is normal rake angle; ϕ_i is oblique shear angle, which is the included angle between shear velocity and the projection of shear velocity on normal plane; ϕ_n is shear angle; θ_i is the included angle between F and the projection of $\phi_n$on normal plane; and θ_n is the included angle between the projection of F on normal plane and Y-axis.

According to the oblique cutting theory [20], the cutting force of oblique cutting can be expressed by Eq. (5):

$$\begin{cases} F_{tc} = F(\cos\theta_i\cos\theta_n\cos\gamma + \sin\theta_i\sin\gamma) = \dfrac{\tau_s bh(\cos\theta_n + \tan\theta_i\tan\gamma)}{[\cos(\theta_n+\phi_n)\cos\phi_i + \tan\theta_i\sin\phi_i]\sin\phi_n} \\ F_{fc} = F\cos\theta_i\sin\theta_n = \dfrac{\tau_s bh\sin\theta_n}{[\cos(\theta_n+\phi_n)\cos\phi_i + \tan\theta_i\sin\phi_i]\sin\phi_n} \\ F_{rc} = F(\sin\theta_i\cos\gamma - \cos\theta_i\cos\theta_n\sin\gamma) = \dfrac{\tau_s bh(\tan\theta_i - \cos\theta_n\tan\gamma)}{[\cos(\theta_n+\phi_n)\cos\phi_i + \tan\theta_i\sin\phi_i]\sin\phi_n} \end{cases} \tag{5}$$

In Eq. (5), ϕ_i, θ_i, ϕ_n, and θ_n satisfy the relation of Eq. (6):

$$\begin{cases} \sin\phi_i = \sqrt{2}\sin\theta_i \\ \cos(\phi_n+\theta_n) = \dfrac{\tan\theta_i}{\tan\phi_i} \end{cases} \tag{6}$$

According to Eq. (5), the coefficient of prediction model is shown in Eq. (7):

$$\begin{cases} K_{tc} = \dfrac{\tau_s(\cos\theta_n + \tan\theta_i\tan\gamma)}{[\cos(\theta_n+\phi_n)\cos\phi_i + \tan\theta_i\sin\phi_i]\sin\phi_n} \\ K_{fc} = \dfrac{\tau_s\sin\theta_n}{[\cos(\theta_n+\phi_n)\cos\phi_i + \tan\theta_i\sin\phi_i]\sin\phi_n} \\ K_{rc} = \dfrac{\tau_s(\tan\theta_i - \cos\theta_n\tan\gamma)}{[\cos(\theta_n+\phi_n)\cos\phi_i + \tan\theta_i\sin\phi_i]\sin\phi_n} \end{cases} \tag{7}$$

In addition, Eq. (8) is true:

$$\begin{cases} \tan(\phi_n+\beta_n) = \dfrac{\cos\alpha_n\tan\gamma}{\tan\eta - \sin\alpha_n\tan\gamma} \\ \tan\beta_n = \tan\beta_a\cos\eta \end{cases} \tag{8}$$

In Eq. (8), $\beta_n = \theta_n + \alpha_n$.

β_n: frictional angle of oblique cutting

β_a: frictional angle of orthogonal cutting

According to Eqs. (6) and (8), Eq. (5) can be turned into Eq. (9):

$$\begin{cases} F_{tc} = \dfrac{bh\tau_s}{\sin\phi_n} \times \dfrac{\cos(\beta_n-\alpha_n) + \tan\gamma\tan\eta\sin\beta_n}{\sqrt{\cos^2(\phi_n+\beta_n-\alpha_n) + \tan^2\eta\sin^2\beta_n}} \\ F_{fc} = \dfrac{bh\tau_s}{\sin\phi_n\cos\gamma} \times \dfrac{\sin(\beta_n-\alpha_n)}{\sqrt{\cos^2(\phi_n+\beta_n-\alpha_n) + \tan^2\eta\sin^2\beta_n}} \\ F_{rc} = \dfrac{bh\tau_s}{\sin\phi_n} \times \dfrac{\cos(\beta_n-\alpha_n)\tan\gamma - \tan\eta\sin\beta_n}{\sqrt{\cos^2(\phi_n+\beta_n-\alpha_n) + \tan^2\eta\sin^2\beta_n}} \end{cases} \tag{9}$$

According to the analysis above, the coefficient of prediction model is shown in Eqs. (10) and (11):

Table 3 The value of δ_i, $\delta_{r,i}$, and hi^* of the left $i_L{}^{th}$ tooth (unit: 0.01mm)

Number of tooth	$i_{L1}{}^{st}$	$i_{L2}{}^{nd}$	$i_{L3}{}^{rd}$	$i_{L4}{}^{th}$	$i_{L5}{}^{th}$	$i_{L6}{}^{th}$	$i_{L7}{}^{th}$	$i_{L8}{}^{th}$	$i_{L9}{}^{th}$	$i_{L10}{}^{th}$	$i_{L11}{}^{th}$	$i_{L12}{}^{th}$	$i_{L13}{}^{th}$
δ_i	–1	–1	0	0	0	0	0	0	1	–1	–2	–2	–2
$\delta_{r,i}$	1	1	0	0	0	0	0	0	-1	1	2	2	2
h_i^*	5	4	5	4	4	4	4	4	5	2	3	4	4

Table 4 The value of δ_i, $\delta_{r,i}$, and hi^* of the middle i^{th} tooth (unit: 0.01mm)

Number of tooth	$i_{M1}{}^{st}$	$i_{M2}{}^{nd}$	$i_{M3}{}^{rd}$	$i_{M4}{}^{th}$	$i_{M5}{}^{th}$	$i_{M6}{}^{th}$	$i_{M7}{}^{th}$	$i_{M8}{}^{th}$	$i_{M9}{}^{th}$	$i_{M10}{}^{th}$	$i_{M11}{}^{th}$	$i_{M12}{}^{th}$	$i_{M13}{}^{th}$
δ_i	1	1	1	5	3	3	2	3	3	3	2	1	0
$\delta_{r,i}$	–1	–1	–1	–5	–3	–3	–2	–3	–3	–3	–2	–1	0
h_i^*	5	4	4	8	2	4	3	5	4	4	3	3	3

$$\text{left tooth}\quad \begin{cases} K_{L,tc} = \dfrac{\tau_s}{\sin\phi_n} \times \dfrac{\cos(\beta_n-\alpha_n)+\tan\gamma\tan\eta\sin\beta_n}{\sqrt{\cos^2(\phi_n+\beta_n-\alpha_n)+\tan^2\eta\sin^2\beta_n}} \\ K_{L,fc} = \dfrac{\tau_s}{\sin\phi_n\cos\gamma} \times \dfrac{\sin(\beta_n-\alpha_n)}{\sqrt{\cos^2(\phi_n+\beta_n-\alpha_n)+\tan^2\eta\sin^2\beta_n}} \\ K_{L,rc} = \dfrac{\tau_s}{\sin\phi_n} \times \dfrac{\cos(\beta_n-\alpha_n)\tan\gamma-\tan\eta\sin\beta_n}{\sqrt{\cos^2(\phi_n+\beta_n-\alpha_n)+\tan^2\eta\sin^2\beta_n}} \end{cases} \tag{10}$$

$$\text{right tooth}\quad \begin{cases} K_{R,tc} = \dfrac{\tau_s}{\sin\phi_n} \times \dfrac{\cos(\beta_n-\alpha_n)+\tan(-\gamma)\tan\eta\sin\beta_n}{\sqrt{\cos^2(\phi_n+\beta_n-\alpha_n)+\tan^2\eta\sin^2\beta_n}} \\ K_{R,fc} = \dfrac{\tau_s}{\sin\phi_n\cos(-\gamma)} \times \dfrac{\sin(\beta_n-\alpha_n)}{\sqrt{\cos^2(\phi_n+\beta_n-\alpha_n)+\tan^2\eta\sin^2\beta_n}} \\ K_{R,rc} = \dfrac{\tau_s}{\sin\phi_n} \times \dfrac{\cos(\beta_n-\alpha_n)\tan(-\gamma)-\tan\eta\sin\beta_n}{\sqrt{\cos^2(\phi_n+\beta_n-\alpha_n)+\tan^2\eta\sin^2\beta_n}} \end{cases} \tag{11}$$

The cutting edge inclination angle of the middle tooth is 0°, which is orthogonal cutting, so the coefficient of the middle tooth can be shown in Eq. (12):

$$\text{middle tooth}\quad \begin{cases} K_{C,tc} = \dfrac{\tau_s\cos(\beta_n-\alpha_n)}{\sin\phi_c\cos(\phi_c+\beta_n-\alpha_n)} \\ K_{C,fc} = \dfrac{\tau_s\sin(\beta_n-\alpha_n)}{\sin\phi_c\cos(\phi_c+\beta_n-\alpha_n)} \end{cases} \tag{12}$$

In Eqs. (10), (11), and (12):

γ: cutting edge inclination angle, known as 2° from Fig. 1

α_n: normal rake angle, which equals to rake angle under orthogonal cutting, known as 8° from Table 1

β_n: frictional angle under oblique cutting

τ_s: shear yield strength

ϕ_n: shear angle

η: chip flow angle, which equals to cutting edge inclination angle, known as 2° from Fig. 1

2.2.2 Identification of parameters in model coefficient

The parameters of β_n,ϕ_n, and τ_s in coefficient of prediction model must be identified before the determination of prediction model. The following analysis is about the solution method of the parameters above:

Frictional angle (β_n) According to the definition of frictional angle, the value of β_n has nothing to do with orthogonal cutting or oblique cutting, which is determined by lubricating condition, knife-chip contact zone status, the material properties, and the features of the tool. Therefore, in the paper, β_n=β_a, and frictional angle only can be obtained by experiment method because mathematical analysis is invalid. It can be known according to geometric relations of cutting theory [20]:

$$\beta_a = \alpha_r + \arctan\frac{F_{fc}}{F_{tc}} \tag{13}$$

In Eq. (13), β_a: frictional angle under orthogonal cutting

α_r: rake angle under orthogonal cutting, known as 8° from Table 1

F_{fc}: normal force under orthogonal cutting

F_{tc}: tangential force under orthogonal cutting

So, β_n can be achieved by the measurement of F_{fc} and F_{tc} under orthogonal cutting.

Normal shear angle (φ_n) According to cutting theory [20], normal shear angle (ϕ_n) equals to shear angle (ϕ_c) of orthogonal cutting. And $\phi_c = \frac{\pi}{4}-(\beta_a-\alpha_r)$ in orthogonal cutting. Therefore, normal shear angle (ϕ_n) can be achieved by frictional angle (β_a) and rake angle (α_r) of orthogonal cutting. α_r is rake angle under orthogonal cutting, known as 8°. Frictional angle (β_a) of orthogonal cutting can be

Table 5 The value of δ_i, $\delta_{r,i}$, and hi^* of the right i^{th} tooth (unit: 0.01mm)

Number of tooth	$i_{R1}{}^{st}$	$i_{R2}{}^{th}$	$i_{R3}{}^{rd}$	$i_{R4}{}^{th}$	$i_{R5}{}^{th}$	$i_{R6}{}^{th}$	$i_{R7}{}^{th}$	$i_{R8}{}^{th}$	$i_{R9}{}^{th}$	$i_{R10}{}^{th}$	$i_{R11}{}^{th}$	$i_{R12}{}^{th}$	$i_{R13}{}^{th}$
δ_i	–	–2	–2	–1	1	1	1	0	0	–1	–1	0	0
$\delta_{r,i}$	4	2	2	1	–1	–1	–1	0	0	1	1	0	0
h_i^*	–	6	4	5	6	4	4	3	4	3	4	5	4

Note: The $i_{R1}{}^{st}$ tooth has been removed, so there is no δ_i and hi^*

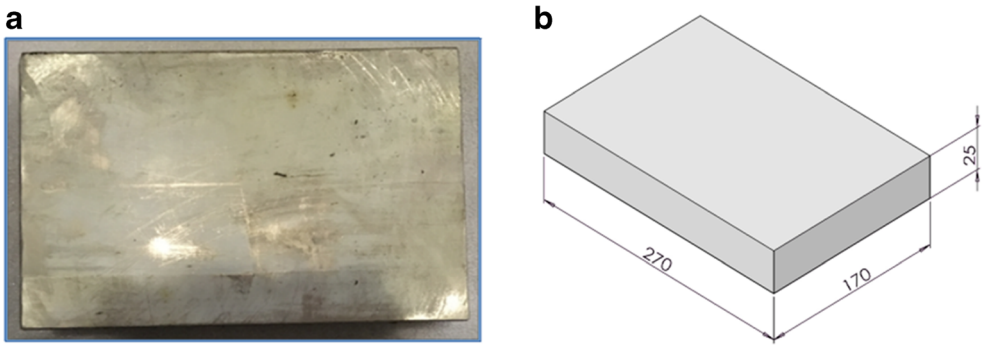

Fig. 6 Titanium alloy specimen. **a** Physical picture of the workpiece. **b** 3D diagram of the workpiece

obtained by cutting experiment, so $\phi_n$can also be obtained by orthogonal cutting experiment.

Shear yield strength (τ_s) Shear yield strength (τ_s) is produced by the cutting stress during machining, which produces a hardened layer on the surface. Shear yield strength (τ_s) is normally bigger than the yield strength of the material itself, which needs to be gained by cutting experiment. The orthogonal cutting experiment is conducted in the study because τ_s has nothing to do with orthogonal cutting or oblique cutting.

In this way, the parameters β_n,ϕ_n, and τ_s are all obtained by orthogonal cutting experiment.

2.3 The determination of cutting output per tooth considering tool runout (h_i^*)

2.3.1 The cause of tool runout

In the study, the disc cutter is made by Zhuzhou Diamond Cutting Tools Co., Ltd., as shown in Fig. 4. The characteristics of the three-teeth alternating disc cutter is consistent with those in Fig. 1. Four cutting edges are symmetrically designed, and each cutting edge has a circular arc chip rolling groove, as shown in Fig. 4c. The size of blade is 12.7×12.7×6 (mm). The workpiece parameters of disc cutter are shown in Table 1; The composition and property of blade are shown in Table 2.

It can be known from Figs. 1 and 4 that the disc cutter is with large diameter and more teeth. There will be an obvious tool runout because of installation error and manufacturing error, namely the distance between each cutting edge and the center of disc cutter is different. The tool runout has an effect on actual cutting output per tooth, which makes a deviation between theoretical value and actual value and then makes the change of milling force. Therefore, the effect of tool runout must be taken into account when milling force model is building. The sketch map of tool runout of disc cutter is shown in Fig. 5 and is indicated in Eq. (14):

$$\delta_i = r_i - \mathrm{R} \tag{14}$$

In Eq. (14):

δ_i: tool runout

r_i: the distance between cutting edge and center of disc cutter

R: cutting radius of disc cutter

2.3.2 The model establishment of cutting output per each considering tool runout (h_i*)

Disc milling is a process of multi-tooth cyclic cutting; if there is no tool runout, the cutting output of next tooth should be the cutting output left by the previous tooth, and the cutting output per tooth should be even. However, the cutting output of the i^{th} tooth may be the allowance left by $(i\text{-}n)^{\mathrm{th}}$ tooth while considering the tool runout, and the cutting output per tooth is uneven. The theoretical value of cutting output per tooth is defined as h_i, and the actual value of cutting output per tooth considering tool runout is defined as h_i*.

A parameter of $\delta_{r,i}$ is introduced before the model is built. $\delta_{r,i}$ is the residual allowance left by the i^{th} tooth, which is the difference value between theoretical surface (Pi) and actual surface (P_{ri}) produced by the i^{th} tooth. It should be noted that the actual surface (P_{ri}) may be not produced by the i^{th} tooth, which may be produced by the $(i\text{-}n)^{\mathrm{th}}$ tooth, because there is

Table 6 Chemical composition of TC17 (mass fraction, %) [21]

Main components					The impurities (not more than)					Margin
Al	Zr	Sn	Mo	Cr	Fe	C	N	H	O	Ti
4.5~5.5	1.5~2.5	1.5~2.5	3.5~4.5	3.5~4.5	0.25	0.05	0.05	0.012	0.08~0.13	/

Table 7 Mechanical properties at normal temperature of TC17 [21]

The status	σ_b(Mpa)	$\sigma_{r0.2}$(Mpa)	δ(%)	ψ (%)
Solution and aging	1180	1110	10	17.5

no allowance for the i^{th} tooth on the account of the tool runout of the i^{th} tooth or the overcut of the $(i\text{-}n)^{th}$ tooth. Take the left-to-right feed direction as an example; if P_{ri} is on the right of P_i, $\delta_{r,i}$ is positive, and if P_{ri} is on the left of P_i, $\delta_{r,i}$ is negative.

Based on the analysis above, the mathematical model in regard to h_i*, h_i, and δ_i is shown in Eq. (15).

$$\begin{cases} h_i^* = h_i + \delta_i + \delta_{r,i-1} & h_i + \delta_i + \delta_{r,i-1} \geq 0 \\ h_i^* = 0 & h_i + \delta_i + \delta_{r,i-1} < 0 \\ \delta_{r,i} = -\delta_i & h_i + \delta_i + \delta_{r,i-1} \geq 0 \\ \delta_{r,i} = h_i + \delta_{r,i-1} & h_i + \delta_i + \delta_{r,i-1} < 0 \end{cases} \quad (15)$$

In Eq. (15), h_i is known, which is 0.04 mm in the experiment.

2.3.3 The measurement of tool runout and determination of h_i^*

It is known from Fig. 1 that the left and right tooth have a cutting edge inclination angle (γ), which leads to the difficulty to measure the tool runout. In the study, in order to measure the tool runout accurately, the following method is adopted: first, a set of teeth is chosen, and the right tooth is marked as $i_{R1}{}^{th}$, the left tooth is marked as $i_{M1}{}^{th}$ tooth, and the mid tooth is marked as $i_{L1}{}^{th}$ tooth. In addition, in order to make the tool runout value one-to-one corresponding to each tooth, the chosen set of right tooth is removed as a mark. Second, the tool runout of $i_{L1}{}^{th}$ tooth is measured by tool setting method, and the tool runout of $i_{L1}{}^{th}$ tooth is denoted as δ_1. Third, make the disc cutter rotate with the speed of 1 r/min, because high rotational speed will cause the vibration of disc cutter to overlay the tool runout and then lead to measurement error of tool runout. In addition, it is difficult to observe the measurement value when the disc cutter rotates with a high speed. Fourth, make the dial gauge to contact with the tool nose, and then measure the relative value of tool runout of each tooth ($\delta_{i\text{-}0}$) with respect to the $i_{L1}{}^{th}$ tooth. Last, the tool runout of each tooth (δ_i) can be obtained by mathematical calculation. There are 13 datasets because the disc cutter has 39 teeth: 13 datasets of the left tooth, 13 datasets of the mid tooth, and 13 datasets of the right tooth. The value of h_i*, $\delta_{r,i}$, and δ_i can be obtained by Eq. (15), as shown in Tables 3, 4, and 5.

2.4 The solution of parameters in prediction model

It can be known from the analysis above that frictional angle (β_n) and shear yield strength (τ_s) are basic parameters, which can be obtained by orthogonal cutting experiment. Normal shear angle (ϕ_n) can be obtained by frictional angle (β_n). Therefore, a series of experiments are conducted. The specific methods are as follows:

2.4.1 Experiment condition and methods

The tool In the study, a disc cutter is used, as shown in Figs. 1 and Fig. 4. We won't go into details.

Materials In the study, titanium alloy TC17 is used, the size is 270×170×25 mm, as shown in Fig. 6. Chemical composition and mechanical properties of TC17 are shown in Table 6 and Table 7, respectively.

It is known that more teeth will participate in cutting at the same time if the workpiece is too thick, which will disturb the experiment data. In order to ensure only one tooth to participate in cutting at the same time, the thickness of workpiece is subject to some limitations, which needs to satisfy Eq. (16):

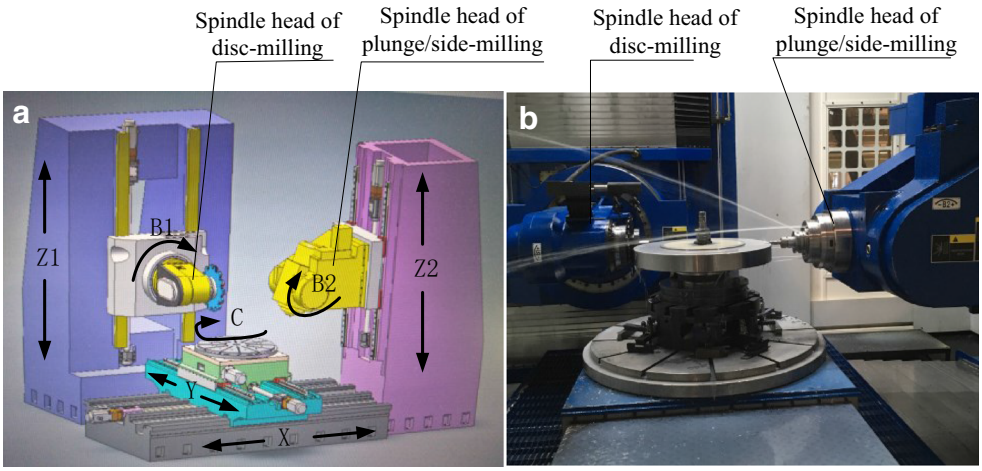

Fig. 7 Disc/plunge/side-milling NC machine tool of blisk

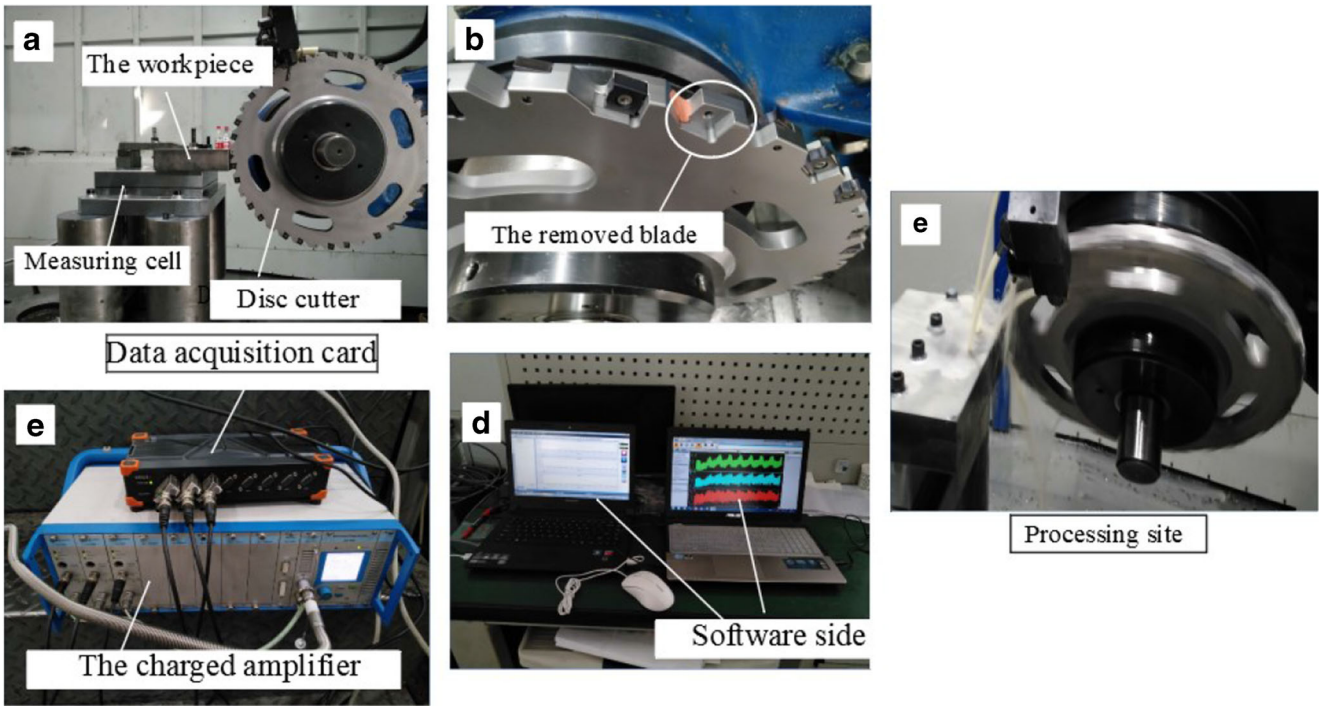

Fig. 8 Experimental picture of milling force meausrement

$$2\arcsin\left(\frac{H}{2R}\right) \le \frac{2\pi}{N} \tag{16}$$

In Eq. (16):
N: the teeth number of the disc cutter
H: the thickness of the workpiece
R: the radius of the disc cutter

The teeth number of the disc cutter is 39, the diameter is 210 mm, and the thickness of the workpiece can be obtained by Eq. (16), which can't be more than 33.9 mm, so the size of titanium alloy workpiece is with the thickness of 25 mm.

Experiment platform Compound efficient NC milling machine tool of aircraft engine blisk is used, which is manufactured by Qinchuan Machine Tool Co., Ltd., as shown in Fig. 7. The machine tool has two spindle head: spindle head of disc milling and spindle head of plunge/side milling. In the study, the spindle head of disc milling is used, whose rated speed is 120 r/min and design torque is 5000 N.m. The parameters in the experiment are as follows: speed of main shaft is 42 r/min, and feed speed is 24 mm/min.

Measurement methods Milling force is measured by a three-way dynamometer. The measuring system consists of a Kistler 9225B dynamic piezoelectric dynamometer, a Kistler 5080 charge amplifier, digital-to-analog conversion device PCIM-DAS1602/1, and DEWESOFT X2 software. The dynamometer is connected to the charge amplifier, and then the charge amplifier is connected to the data acquisition card, so milling force in three directions is recorded by DEWESOFT X2 software, as shown in Fig. 8 and Fig. 9. F_r is lateral force defined as X direction, F_f is normal force defined as Y direction, and F_t is tangential force defined as Z direction. The processing axis system and the measurement axis system are

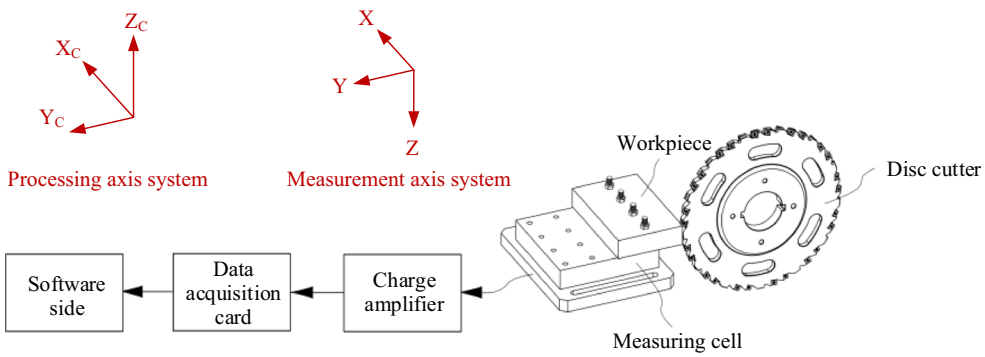

Fig. 9 The measurement schematic diagram of milling force

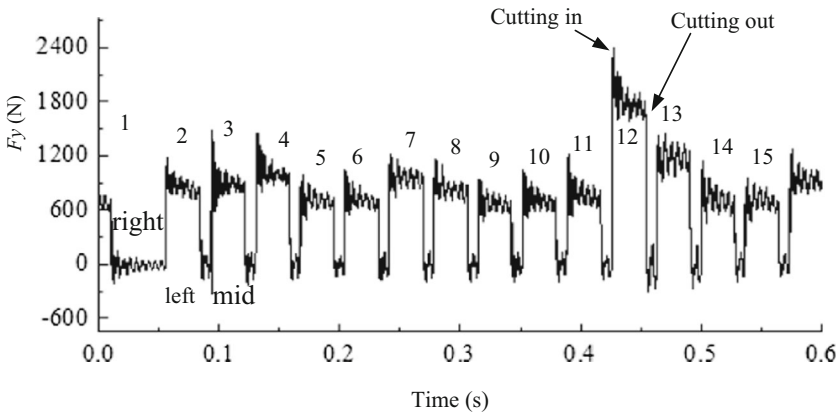

Fig. 10 Cutting force curve of Y direction

shown in Fig. 9. It shows that the X-axis and Y-axis of both are in the same direction, and the Z-axis is opposite.

It is known from the analysis above that the parameters of prediction model (β_n, ϕ_n, τ_s) can be obtained by orthogonal cutting experiment, so only the middle tooth is chosen as research object because the left tooth and right tooth are oblique cutting. The recorded curve of milling force cannot correspond with the cutter teeth one to one because the disc cutter has too many teeth, so the curve of milling force needs to be marked. The specific method is the same as the measurement method of tool runout, namely the same right tooth is removed as well as the measurement of tool runout. In this way, the curve of milling force and tool runout can correspond to the tooth one to one, as shown in Fig. 8b. The cutting output of the removed right tooth leaves to the next tooth, so there is a trough of wave corresponding to this tooth, and a peak of wave occurs corresponding to the next tooth. In this way, the curve of milling force can correspond to each tooth.

2.4.2 The solution of frictional angle (β_n)

The frictional angle (β_n) is displayed in Eq. (17):

$$\beta_n = \beta_a = \alpha_r + \arctan\frac{F_{fc}}{F_{tc}} \tag{17}$$

In Eq. (17):

β_a: frictional angle under orthogonal cutting

α_r: rake angle under orthogonal cutting, known as 8°

F_{fc}: normal force

F_{tc}: tangential force

It is known from Eq. (17) that frictional angle (β_n) can be achieved by the measurement of F_{fc} and F_{tc}. Therefore, only normal force (F_{fc}) and tangential force (F_{tc}) are considered in the study. The measurement result of $F_y(\theta)$ and $F_z(\theta)$ by the dynamometer is expressed in Eq. (18); the F_{fc} and F_{tc} can be gained by Eq. (19).

$$\begin{cases} F_y(\theta) = F_{tc}\sin\theta + F_{fc}\cos\theta \\ F_z(\theta) = F_{tc}\cos\theta + F_{fc}\sin\theta \end{cases} \tag{18}$$

$$\begin{cases} F_{fc} = F_y(\theta)\cos\theta + F_z(\theta)\sin\theta \\ F_{tc} = F_y(\theta)\sin\theta + F_z(\theta)\cos\theta \end{cases} \tag{19}$$

The curve of milling force in Y and Z direction is recorded in Fig. 10 and Fig. 11. The trough of wave 1 is produced by the removed right tooth, so the peak of waves 3, 6 ,9, 12, and 15 is produced by the middle tooth. There is an impact when the disc cutter cuts into the workpiece because disc milling is a typical discontinuous cutting, which leads to unstable data, so the data of cutting-in cannot be used for analysis. The data of cutting-out is relatively more stable and can be used in the

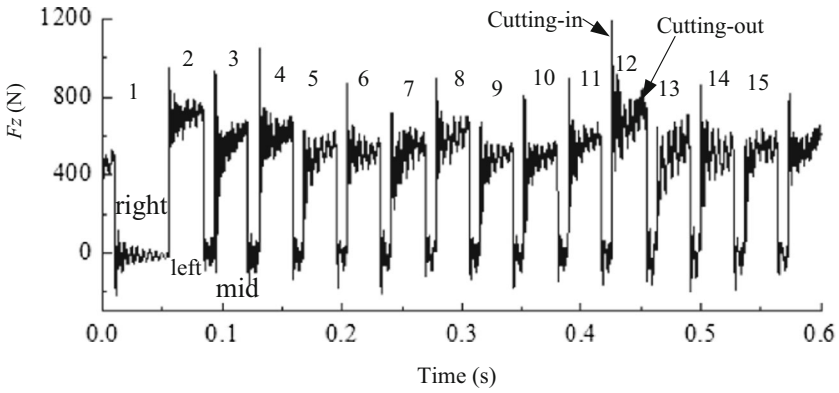

Fig. 11 Cutting force curve of Z direction

Table 8 The value of milling force of 5 middle teeth in direction Y and Z while cutting-out

Tooth number	#3	#6	#9	#12	#15
$F_y(N)$	881.3	716.1	678.7	1739.4	690.9
$F_z(N)$	671.5	581.2	567.5	846.8	600.1

Table 9 The results of F_{fc}, F_{tc}, F_{fc}/F_{tc}, and arctan F_{fc}/F_{tc}

Number of tooth	#3	#6	#9	#12	#15
$F_{fc}(N)$	618.1	537.7	526.2	739.4	558.1
$F_{tc}(N)$	919.5	749.3	711.2	1786.5	725.3
F_{fc}/F_{tc}	0.67	0.72	0.74	0.41	0.77
arctan (F_{fc}/F_{tc})	33.8°	35.8°	36.5°	22.3°	37.6°

Table 10 The data of F_s

Number of tooth	#3	#6	#9	#12	#15
$F_s(N)$	1566.6	1304.1	1250.9	2733.9	1294.1

study. The values of F_y and F_z of waves 3, 6 ,9, 12, and 15 are shown in Table 8.

In the study, the thickness of specimen is 25 mm, so the value of θ is obtained by Eq. (20):

$$\theta = -\arcsin\frac{\mathrm{H}}{\mathrm{R}} = -\arcsin\frac{25}{2\times 210} = -3.4° \tag{20}$$

The value of F_y, F_z, and θ are put into Eq. (19), and then the value of F_{fc} and F_{tc} is gained, as shown in Table 9. Then, the value of F_{fc}/F_{tc} and arctan F_{fc}/F_{tc} is gained, as also shown in Table 9.

It is known from Table 9 that the value of milling force of #12 is much bigger than that of others, which is due to the blade installation without fastening, and leads to the abnormal value of milling force, so the data needs to be removed. The mean value of arctan (F_{fc}/F_{tc}) excluding #12 data is shown in Eq. (21) (Zhao and Fu, 2020).

$$\overline{\arctan\left(F_{fc}/F_{tc}\right)} = 35.9° \tag{21}$$

It is known that α_r is 8°, so frictional angle (β_a) can be obtained by Eq. (22):

$$\beta_n = \beta_a = \alpha_r + \arctan\left(\frac{F_{fc}}{F_{tc}}\right) = 43.9° \tag{22}$$

2.4.3 The solution of normal shear angle (φ_n)

It is known from the analysis above that $\phi_n = \phi_c$, and $\phi_c = \frac{\pi}{4} - (\beta_a - \alpha_r)$. Known from Eq. (22), $\beta_n = \beta_a = 43.9°$, and $\alpha_r = 8°$, so normal shear angle $\phi_n = \phi_c = \frac{\pi}{4} - (\beta_a - \alpha_r) = 9.1°$.

2.4.4 The solution of shear yield strength (τ_s)

Known from the definition of τ_s, which equals to the ratio of yield stress to shear plane area, as shown in Eq. (23):

$$\tau_s = \frac{F_s}{A_s} \tag{23}$$

In Eq. (23), F_s is shear force, which equals to the projection of resultant force (F_c) on shear plane. Equation (24) can be achieved according to the cutting principle and principle of maximum shear stress. So, the F_s can be gained through Eq. (24) and the data of Table 9, as shown in Table 10.

$$F_s = F_c\cos(\phi_c + \beta_a - \alpha_r) = F_c\cos\frac{\pi}{4} = \frac{\sqrt{2}}{2}\times\sqrt{F_{tc}^2 + F_{fc}^2} \tag{24}$$

In Eq. (23), A_s is shear surface area, which satisfies Eq. (25). Known from Section 2.3.3, $\phi_c = 9.1°$. So, substitute ϕ_c into Eq. (25), and then A_s can be obtained, as shown in Eq. (26).

$$A_s = b\frac{h_{\mathrm{i}}^*}{\sin\phi_c} \tag{25}$$

$$A_s = 6.332\times bh_{\mathrm{i}}^* \tag{26}$$

In Eq. (26), b is the width of cutting edge, known to be 6 mm. h_i* is the cutting output per tooth considering tool runout, known from Table 4. Therefore, A_s is obtained, and then τ_s is obtained, as shown in Table 11.

Table 11 The value of shear surface area and shear yield strength

Number of tooth	#3	#6	#9	#12	#15
$A_s(mm^2)$	1.8996	1.5197	1.5197	3.0394	0.7598
$\tau_s(Mpa)$	824.6999	858.1299	823.1230	899.4867	1703.2114

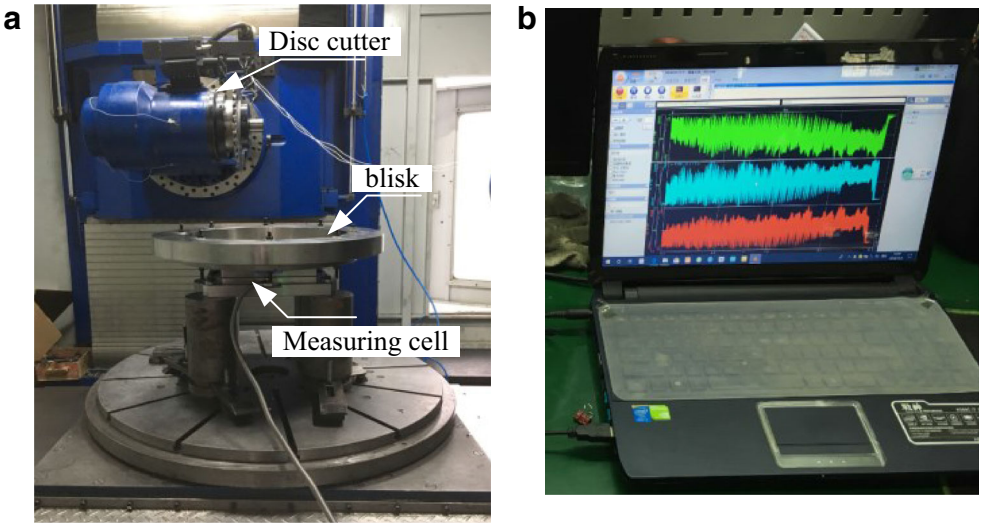

Fig. 12 Verification experiment: **a** the processing site and **b** the waveform acquisition

Table 12 Processing parameters and the size of blisk

The size of blisk	Material	Speed of mainshaft (r/min)	Feed speed (mm/min)	Cutting state
(ϕ640××25 mm)	TC17	42	24	One-tooth
(ϕ640×50 mm)	TC17	58	28	Two-teeth

It is can be seen from Table 11 that the data of #15 is inconsistent with others, which may be produced by tool runout, so should be removed. Then, the mean value of τ_s is obtained by Eq. (27).

$$\overline{\tau_s} = \frac{1}{4}\sum_{i=1}^{4}\tau_{s,i} = 851.3599 \tag{27}$$

The prediction model of milling force can be obtained according to the solution of parameters above, as shown in Eq. (28).

$$\begin{cases} \sum F_{Qt,i}(\theta) = F_{Lt,i}(\theta) + F_{Ct,i+1}(\theta) + F_{Rt,i+2}(\theta) \\ \sum F_{Qf,i}(\theta) = F_{Lf,i}(\theta) + F_{Cf,i+1}(\theta) + F_{Rf,i+2}(\theta) \\ \sum F_{Qr,i}(\theta) = F_{Lr,i}(\theta) + F_{Cr,i+1}(\theta) + F_{Rr,i+2}(\theta) \end{cases} \tag{28}$$

3 The verification of prediction model

In order to verify the validity of the prediction model, the experiment of disc milling is designed. The tool, machine tool, and measurement system of milling force are consistent with the previous experiment, which will not be detailed here; the picture of the verification experiment is shown in Fig. 12. In the verification experiment, the blisk with two different thicknesses are chosen: 25 mm and 50 mm. One tooth participates in the cutting when the thickness is 25 mm, and two teeth participates in the cutting when the thickness is 50 mm, so the validity of the model under different cutting conditions can be verified. The size of blisk and processing parameters

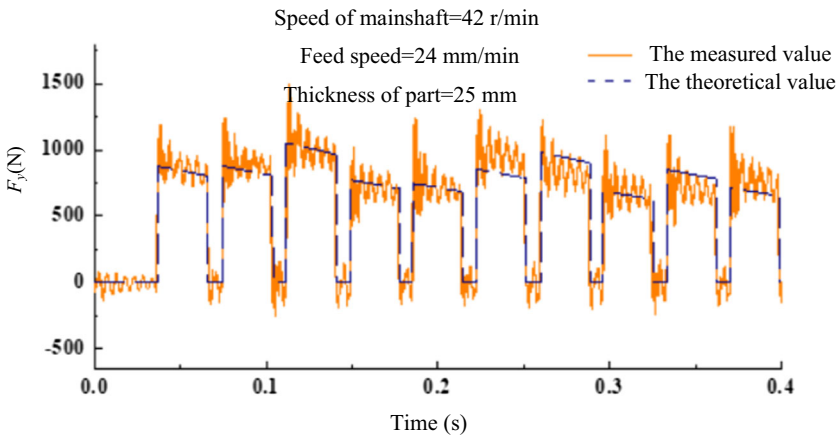

Fig. 13 Milling force contrast curve of Y direction of one-tooth cutting condition

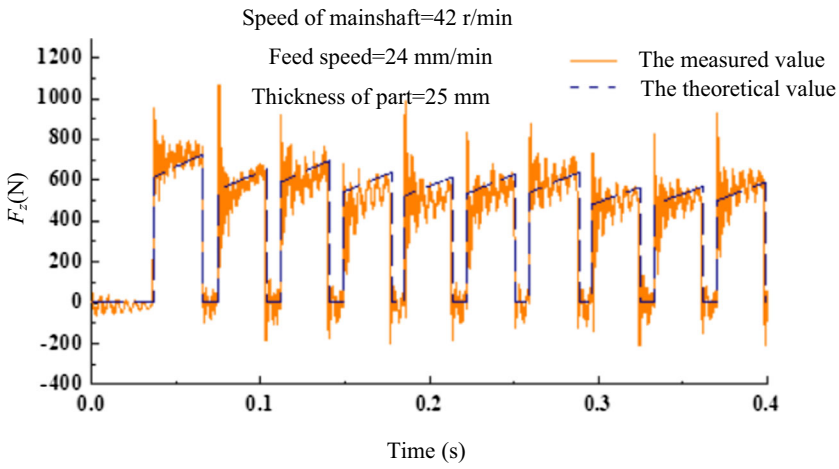

Fig. 14 Milling force contrast curve of Z direction of one-tooth cutting condition

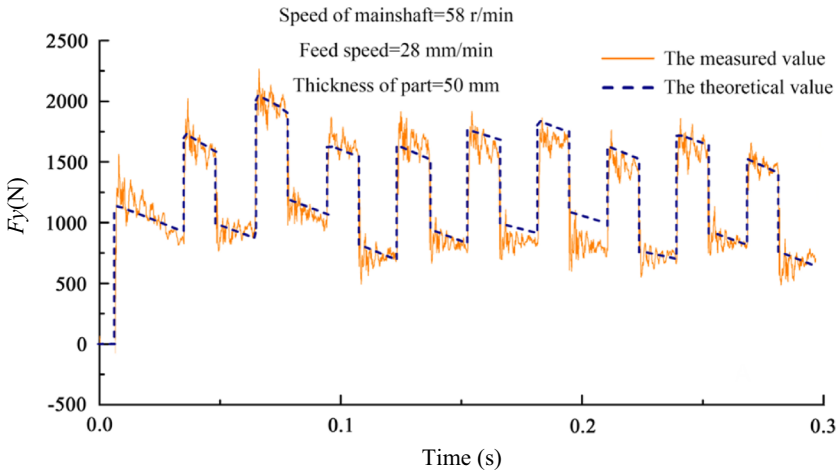

Fig. 15 Milling force contrast curve of Y direction of two-teeth cutting condition

are shown in Table 12. Chemical composition and mechanical properties of TC17 are shown in Table 6 and Table 7 respectively.

The contrast curve of predicted value and actual value of milling force under one-tooth cutting condition is indicated in Fig. 13 and Fig. 14. The contrast curve of two-teeth cutting is shown in Figs. 15 and 16. It can be known from Figs. 13–16 that the model is with high efficiency and precision and the measured force and predictive force are in good agreement in amplitude and trend. So, the predictive model of milling force

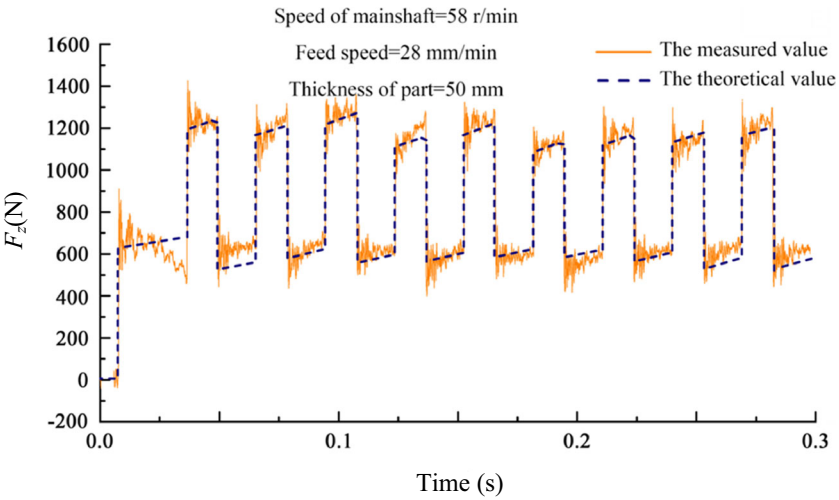

Fig. 16 Milling force contrast curve of Z direction of two-teeth cutting condition

can be used in the study of milling force of disc milling in the blisk. The exact prediction of milling force will provide powerful support to the study of vibration, temperature, tool wear, surface quality, and others.

4 Conclusion

(1) In the study, the prediction model of disc milling force is established considering tool runout with a three-teeth alternating disc cutter. In order to measure tool runout accurately, the disc cutter is revolving with low speed, which is 1 r/min, and the mathematical model in regard to cutting output per tooth considering the tool runout (h_i^*), cutting output per tooth (h_i), and tool runout (δ_i) is set up. Then, cutting output per tooth considering the tool runout (h_i^*) is obtained by the mathematical model.

(2) The parameters (β_n, ϕ_n,τ_s) in the prediction model are resolved by orthogonal cutting experiment. The verification experiment shows that the prediction model established by this method is with high efficiency and precision and the measured force and predictive force are in good agreement in amplitude and trend whether in one-tooth cutting condition or two-teeth cutting condition.

Acknowledgements This work was supported by the Project Funded by the National Numerical Control Major Projects Foundation of China (Grant No. 2013ZX04001081), China Postdoctoral Science Foundation (Grant No: 2018M631195). Hubei Superior and Distinctive Discipline Group of Mechatronics and Automobiles (Grant No: XKQ2021013).

Availability of data and materials The data sets supporting the results of this article are included within the article and its additional files.

Author contribution The experiment is designed and carried out mainly by Yang Cheng. The experiment equipment and funding is done by Shi Yaoyao. The writing in English is done by Xin Hongmin. Zhang Nan participated in the experiment as Yang Cheng's assistant.

Declarations

Ethics approval and consent to participate The research does not involve human participants and/or animals.

Consent for publication The publication has been approved by all authors.

Competing interests The authors declare no competing interests.

References

1. Xin HM, Shi YY, Wu HW, Zhao T, Yang F, Wang L (2020) Tool wear in disc milling grooving of aircraft engine blisk. Iran J Sci Technol Transact Mechan Engine 1:315–323. https://doi.org/10.1007/s40997-019-00338-4
2. Feng ZX, Liu M, Li GH (2019) Identification of polynomial cutting coefficients for a dual-mechanism ball-end milling force model. Recent Patents Eng 13(3):232–240. https://doi.org/10.2174/1872212112666180629142036
3. Wei ZC, Guo ML, Wang MJ, Li SQ, Liu SX (2018) Force predictive model for five-axis ball end milling of sculptured surface. Int Adv Manufact Technol 98(5-8):1367–1377. https://doi.org/10.1007/s00170-018-2125-4
4. Lu XH, Wang FR, Jia ZY, Si L, Zhang C, Liang SY (2017) A modified analytical cutting force prediction model under the tool flank wear effect in micro-milling nickel-based superalloy. Int J Adv Manuf Technol 91(9-12):3709–3716. https://doi.org/10.1007/s00170-017-0001-2
5. Hou YF, Zhang DH, Wu BH, Luo M (2015) Milling force model of worn tool and tool flank wear recognition in end milling. IEEE/ASME Trans Mechatr 20(3):1024–1035. https://doi.org/10.1109/TMECH.2014.2363166
6. Song QH, Liu ZQ, Ju GG, Wan Y (2019) A generalized cutting force model for five-axis milling processes. Proceed Instit Mechan Eng B 233(1):3–17. https://doi.org/10.1177/0954405417711970
7. Li SP, Tian LC Qin XD, et al (2017) Diameter error compensation based on flexible cutting force model in hole helical milling process. Tianjin Daxue Xuebao 50(2):147-153. DOI: 10.11784/tdxbz201512083
8. Stemmler S, Abel D, Schwenzer M, Adams O, Klocke F (2017) Model predictive control for force control in milling. IFAC-Papersonline 50(1):15871–15876. https://doi.org/10.1016/j.ifacol.2017.08.2336
9. Zhang T, Liu ZQ, Xu CH (2015) Theoretical modeling and experimental validation of specific cutting force for micro end milling. Int J Adv Manuf Technol 77(5-8):1433–1441. https://doi.org/10.1007/s00170-014-6549-1
10. Niu ZC, Cheng K (2020) Improved dynamic cutting force modeling in micro milling of metal matrix composites part I: theoretical model and simulations. Proceed Instit Mechan Eng C 234(9):1733–1745. https://doi.org/10.1177/0954406219899688
11. Cai LG, Pu FY, Zhao YS (2012) Milling force modeling of formed milling cutter for turnout processing and experiment validation. Adv Mater Res 538-541:921–926. https://doi.org/10.4028/www.scientific.net/AMR.538-541.921
12. Guo ML, Wei ZC, Wang MJ, Li S, Liu S (2018) An identification model of cutting force coefficient for five-axis ball-end milling. Int Adv Manufact Technol 99(1-4):937–949. https://doi.org/10.1007/s00170-018-2451-6
13. Guo ML, Wei ZC, Wang MJ et al (2019) Force prediction model for five-axis flat end milling of sculptured surface. J Mechan Eng 55(7):225–233
14. Zhang Y, Li S, Zhu KP (2020) Generic instantaneous force modeling and comprehensive real engagement identification in micro-milling. Int J Mech Sci 176(15):110–118. https://doi.org/10.1016/j.ijmecsci.2020.105504
15. Fu ZT, Yang WY, Wang XL, Leopold J (2016) An analytical force model for ball-end milling based on a predictive machining theory considering cutter runout. Int J Adv Manuf Technol 84(9-12):2449–2460. https://doi.org/10.1007/s00170-015-7888-2
16. Zhuang KJ, Zhu DH, Ding H (2018) An analytical cutting force model for plunge milling of Ti6Al4V considering cutter runout. Int J Adv Manuf Technol 94(9-12):3841–3852
17. Li G, Qu D, Feng WW et al (2016) Modeling and experimental study on the force of micro-milling titanium alloy based on tool runout. Int J Adv Manuf Technol 87(1-4):1193–1202. https://doi.org/10.1007/s00170-017-1078-3
18. Xin HM, Shi YY, Ning LQ (2017) The influence of thermal-mechanical coupling on surface integrity in disc milling grooving

of titanium alloy. Mach Sci Technol 21(2):313–333. https://doi.org/10.1080/10910344.2017.1284561
19. Zhang N, Shi YY (2019) A 3-D instantaneous cutting force prediction model of indexable disc milling cutter for manufacturing blisk-runnels considering runout. Int J Adv Manuf Technol 103(9-12): 4029–4039. https://doi.org/10.1007/s00170-019-03780-5
20. Altintas Y (2012) Manufacturing automation: metal cutting mechanics, machine tool vibrations, and CNC design. Cambridge University Press, London
21. Zhao PK, Fu L (2020) Numerical and experimental investigation on power input during linear friction welding between TC11 and TC17 alloys. J Mater Eng Perform 29(4):2016–2072. https://doi.org/10.1007/s11665-020-04745-6